Philosophical Magazine

ISSN: (Print) (Online) Journal homepage: https://www.tandfonline.com/loi/tphm20

Graphite to AlB_2 and MgB_2: a comparative study of their tight-binding model and Dirac nodal line

Cai Cheng, Man-Yi Duan, Wen-Xuan Xu, Zhao Wang & Xiao-Lin Zhou

To cite this article: Cai Cheng, Man-Yi Duan, Wen-Xuan Xu, Zhao Wang & Xiao-Lin Zhou (2021): Graphite to AlB_2 and MgB_2: a comparative study of their tight-binding model and Dirac nodal line, Philosophical Magazine, DOI: 10.1080/14786435.2021.1978575

To link to this article: https://doi.org/10.1080/14786435.2021.1978575

PHILOSOPHICAL MAGAZINE
https://doi.org/10.1080/14786435.2021.1978575

Taylor & Francis
Taylor & Francis Group

Graphite to AlB_2 and MgB_2: a comparative study of their tight-binding model and Dirac nodal line

Cai Cheng [a,b], Man-Yi Duan[a], Wen-Xuan Xu[a], Zhao Wang[a] and Xiao-Lin Zhou[a]

[a]School of Physics and Electronic Engineering, Sichuan Normal University, Chengdu, People's Republic of China; [b]School of Materials and Energy, State Key Laboratory of Electronic Thin Film and Integrated Devices, University of Electronic Science and Technology of China, Chengdu, People's Republic of China

ABSTRACT

Recently, the AlB_2-type compounds such as AlB_2 and MgB_2 have attracted immense interest due to the Dirac Nodal Line (DNL). This unique electronic structure is very important for the design and discovery of topological superconductivity, but the DNL of AlB_2-type compounds has not been unambiguously comparative studied. Here, we systematically investigated the electronic topological properties of AlB_2 and MgB_2 by tight-binding model analysis and first-principles calculations. The Slater–Koster method fitted band structure results showed that the slope of σ-bond in Γ-A direction was mainly controlled by the absolute value of $V_{ppπ}$. Moreover, the band structure fitted by two p_z Symmetry-Adapted Wannier Function (SAWF) was consistent with the band structure obtained by the effective Hamiltonian of two orbital. In the constructed effective Hamiltonian, the external on-site energies in MgB_2 and AlB_2 were 0.075 and 2.47 eV, respectively, which were mainly due to the distance between Fermi level and Dirac point at the high-symmetry K and H points. More strikingly, it was found that the degree of bending of the topological surface state was related to the number of the selected orbits, and the larger the number of orbits, the stronger the degree of bending. This important finding might be due to the asymmetry of the crystal structure and band structure. This work provides a meaningful reference for exploration of the topological property of DNL in AlB_2-type topological superconductivity materials.

ARTICLE HISTORY
Received 3 June 2021
Accepted 6 July 2021

KEYWORDS
AlB_2-type materials; Symmetry-Adapted Wannier Function; Tight-Binding Model; Dirac Nodal Line; Effective Hamiltonian

CONTACT Cai Cheng ccheng@sicnu.edu.cn School of Physics and Electronic Engineering, Sichuan Normal University, Chengdu 610101, People's Republic of China

Supplemental data for this article can be accessed doi:10.1080/14786435.2021.1978575.

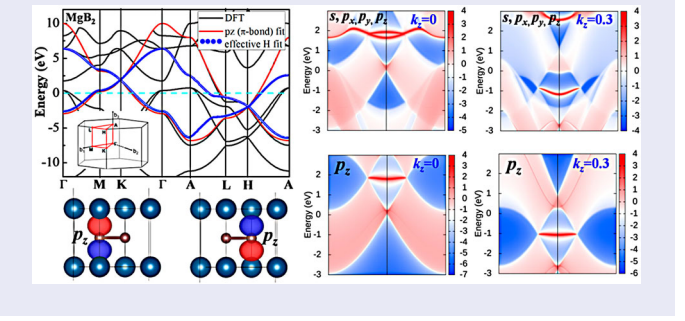

1. Introduction

In the extensive research on topological insulators, the topological semimetals and topological superconductors in electronic structures [1–4] and the topological properties in the phonon dispersion curves [5–9] have recently attracted attention in the fields of condensed matter physics and materials science. MgB_2 has a superconducting transition temperature T_c (39 K) under the theoretical limit of BCS theory, which is currently the highest superconducting transition temperature among binary compounds [10,11]. Topological and superconducting states are intriguing and elusive quantum phenomena in nature. How to integrate topological and superconducting states in the same real solid material system is a frontier issue of current research, such as Majorana fermions. Recently, Jin et al. [12] predicted that MgB_2 exhibited a unique one-dimensional dispersive Dirac Nodal Line (DNLs). Subsequently, Angle-resolved Photoemission Spectroscopy (ARPES) was used to observe the corresponding topological surface states (TSS's) of MgB_2 [13]. Moreover, the existence of DNLs is also observed on the electronic band structure in the similar structure of AlB_2 [14]. In addition, in similar AlB_2-type institutions such as TiB_2 and ZrB_2, there also exists DNLs on their band structure [15]. DNLs also exist in some other materials, such as Pure Alkali Earth Metals of Be, Mg, Ca, Sr and ZrGeSerese, etc. [16–21]. Furthermore, Li et al. [22] predicted the Phononic Weyl Nodal Straight Lines (PTWNLs) on phonon spectrum of MgB_2, which triggered an upsurge in the study of phonon dispersion in high superconducting superconductors.

As all we known, the higher superconducting transition temperature of MgB_2 is mainly due to the strong electron–phonon coupling interaction between the electron near the fermi level and the phonon with E_{2g} mode [23,24]. At the same time, the σ-bond provides a large amount of electrons near the Fermi level. The topological nature of the DNLs above discussions is derived from the π-band. How to separate the π-band and the σ-bond, and use the corresponding model for separate analysis and research is very important. This question has not been solved, and nobody has investigated this issue systematically and comparatively. This is the part motivation of our researches. Here, we systematically

investigated the electronic topological properties of AlB_2-type system (AlB_2 and MgB_2) by tight-binding model analysis and first-principles calculations.

In this work, we proposed that the slope of σ-bond in Γ-A direction was mainly controlled by the absolute value of $V_{pp\pi}$ by the Slater–Koster method fitted band structure results. In the constructed effective Hamiltonian, since the difference between Fermi level relative to the Dirac point at the highly symmetrical K and H points, the external on-site energies in MgB_2 and AlB_2 are 0.075 and 2.47 eV, respectively. More strikingly, it was found that the degree of bending of the TSS was related to the number of selected orbitals, and the more orbitals, the stronger the degree of bending. In essence, the more orbitals, the more accurately fitted the band structure obtained by first-principles calculations. This important finding might be due to the asymmetry of the crystal structure and band structure. This work has deepened the understanding of the degree of surface state curvature in the DNL topological properties of AlB_2-type topological superconductivity materials.

2. Methods

The first-principles calculations were performed by using the Vienna *ab*-initio simulation package (VASP) [25–27]. The Projector-augmented-wave (PAW) was adopted [28] to take into account the electron–ion interactions. The generalized gradient approximation (GGA) [29] in the form of Perdew–Burke–Ernzerhof function was used to exchange–correlation interactions. A self-consistent field method (tolerance 10^{-5} eV/atom) was employed in conjunction with plane wave basis sets of cutoff energy of 500 eV. The Γ-centered with 24 × 24 × 24 *k*-mesh was used to sample the Brillouin zone. The TSSs associated with the (010) surface were calculated by using WannierTools [30].

3. Results and discussion

3.1 Crystal structure and electronic properties

AlB_2-type classes crystallize is a hexagonal lattice system with the P6/mmm (No. 191, D_{6h}) space group. Al and B atoms occupy the (0.0, 0.0, 0.0) and (1/3, 2/3, 1/2) sites, respectively. The optimized lattice constants of AlB_2 are $a = b = 3.011$ Å and $c = 3.285$ Å, and the optimized lattice constants of MgB_2 are $a = b = 3.073$ Å and $c = 3.507$ Å, which are very close to the experimental values [31] and theoretical values [32]. The following results shown are based on optimized lattice constants. Figure 1(a) shows the calculated fat band structures and the corresponding partial density of state (PDOS) of bulk MgB_2 without spin-orbital coupling (SOC). The crystal structure and

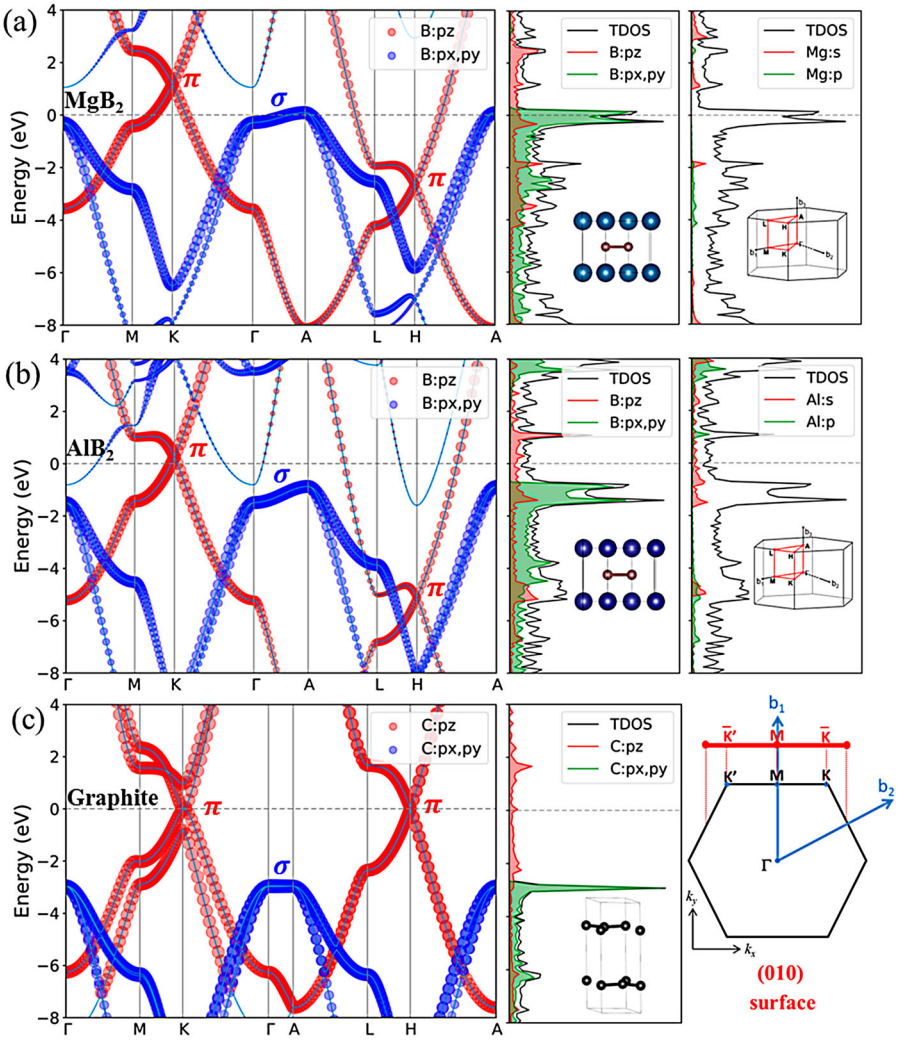

Figure 1. Fat band structure and partial density of state (PDOS) of bulk MgB_2, AlB_2 and Graphite, respectively. (a,b) The fat band structure projected by p_z (π-bond, red colour) and p_x+p_y (σ-bond, blue colour) orbit of B atom, the partial density of states (PDOS) of Mg (Al) and B atom. (c) The fat band structure projected by p_z (π-bond, red colour) and p_x+p_y (σ-bond, blue colour) orbit of C atom, the partial density of states (PDOS) of C atom. The insert figures are the crystal structure, Brillouin zone and (010) Surface, respectively.

the corresponding Brillouin zone (BZ) are shown in the insert illustrations of PDOS, where the high-symmetry points and lines are indicated by red colour. It can be clearly seen from Figure 1(a) that there are Dirac cones at K and H points, which are mainly composed by p_z orbital (π-bond, red colour) of B atoms. The flat bands in ΓA direction are mainly composed by p_x+p_y orbitals (σ-bond, blue colour) of B atoms. There are also six holes and electron pockets at high-symmetry K and H points, respectively. The fat bands with a wider energy range are shown in Figure S1. Figure S1(a–d)

shows that the fat band structure and size of spectral weight are projected by *s* orbit of Mg atom and *p* orbit of B atom, respectively. The calculated fat band structures and the corresponding PDOS of bulk AlB_2 without SOC were shown in Figure 1(b). The fat band structures and PDOS of AlB_2 are similar to that of MgB_2. The striking difference is the position of the σ-bond, which contributes greatly to the Fermi level density of states due to the two dimensionality. The position of the σ-bond in AlB_2 is far away from Fermi level and is completely filled. In contrast, MgB_2 is relatively close to or even beyond the Fermi level. The bands across the fermi level indicate that MgB_2 has stronger metallicity, which also can be obtained from the PDOS near the Fermi level. Moreover, there is a subtle difference, such as the σ-bond of MgB_2 and AlB_2 have a different slope in ΓA direction. The fat bands with a wider energy range of AlB_2 are shown in Figure S2. For comparison, we also calculated the fat band structures and the corresponding PDOS of Graphite as shown in Figure 1(c). From the figures, we know that the position of the Dirac point at point K and H of Graphite is 0. Note that the position of the Dirac point at point K and H are indicated by ε_D^K and ε_D^H, respectively. For the MgB_2, the $\varepsilon_D^K = 1.83$ eV and $\varepsilon_D^H = -1.98$ eV. However, the $\varepsilon_D^K = 0.25$ eV and $\varepsilon_D^H = -5.19$ eV in AlB_2. The energy difference between the K and H points demonstrates the degree of symmetry with respect to the Fermi level. Moreover, it is reasonable for us to artificially introduce on-site energy in the following, which can make the two-band model fitted the band structure better.

3.2 Maximally-localised Wannier functions (MLWFs) and Slater–Koster tight-binding method

Using the linear combination of atomic orbitals (LCAO) method, a set of non-interacting single particles can be used to describe the system. In order to better obtain the basic characteristics of the electronic band structure, we use two kinds of tight-binding models to fit the band structure. One method is to use the Hamiltonian of the tight-binding model generated by nine Wannier orbits (Mg/Al:*s*, B:*s*, p_x, p_y, p_z), which is suitable for using the MLWF to reproduce the PBE energy band structure. The fitted band structure is shown as the red line in Figure 2. Judging from the black and red lines, the band structure fits very well. The other method is Slater–Koster method. The Slater–Koster method [33] is also a powerful way to reproduce the first-principles calculated data. Here, we used Tight-Binding Studio (TB Studio) software package [34,35] to reproduce the Hamiltonian and the overlap matrix elements. The calculate integrals on the whole unit cell and the orbitals *s*, p_x, p_y, and p_z, respectively. The expected values of four integrals ($V_{ss\sigma}$, $V_{sp\sigma}$, $V_{pp\sigma}$, $V_{pp\pi}$) of the Hamiltonian based on the

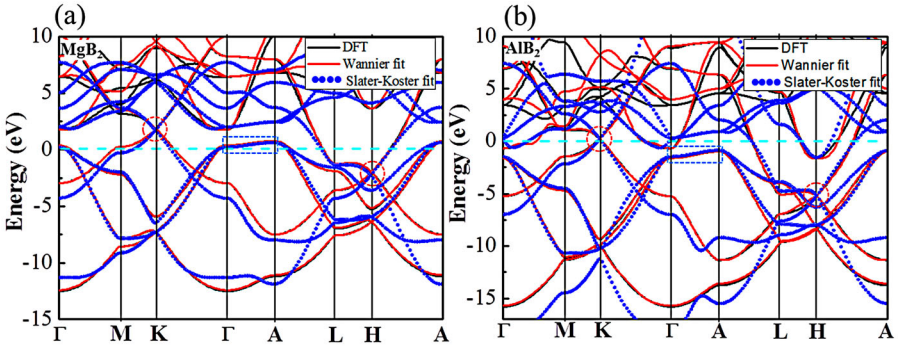

Figure 2. The band structure fitted by Maximally-Localised Wannier Functions (MLWFs) and Slatter-Koster tight-binding method. (a,b) The calculated band structure, Maximum Localised Wannier Function (MLWF) fitted band structure (solid line with red colour), Slatter-Koster tight-binding method fitted band structure (dotted line with blue colour). The *s* orbit of metal atom (Al/Mg) and *s*, p_x, p_y, p_z orbit of B atom fitted in MLWF and Slater–Koster tight-binding method.

directed orbitals as follows:

$$\langle s|H|s\rangle = V_{ss\sigma}$$

$$\langle s|H|p_i\rangle = n_i V_{sp\sigma}$$

$$\langle p_i|H|p_j\rangle = (\delta_{ij} - n_i n_j)V_{pp\pi} + n_i n_j V_{pp\sigma}$$

where $n_i = r \cdot e_i/|r|$ is the directional cosine, r is the vector along the bond, and i takes x, y, and z. For example, the schematic diagram of hopping parameters of the Slater–Koster method for MgB_2 is shown in Figure S3. There are four types of bonds, three Mg–Mg bonds in plane, twelve Mg–B bonds, three B–B bonds in plane, two B–B bonds out plane. In this work, the TB parameters are obtained by fitting the electronic band structure of MgB_2 and AlB_2 calculated by first principles. In Table 1, we list the SK parameters of bond type by fitting DFT energy bands as the shown blue dotted line in Figure 2. As we all know that the σ-band basically has a strong two dimensionality (small

Table 1. The Slater–Koster parameters are obtained by fitting MgB_2 (top) and AlB_2 (bottom). The *V* parameters are in eV.

MgB_2	$V_{ss\sigma}$	$V_{sp\sigma}$	$V_{pp\sigma}$	$V_{pp\pi}$
bond $_{(Mg–Mg)}$	−0.2	–	–	–
bond $_{(B–B\ in\ plane)}$	−2.5	−3.0	1.4	−2.0
bond $_{(B–B\ out\ plane)}$	−0.5	−0.5	1.0	−0.10
bond $_{(Mg–B)}$	−0.5	−1.2	–	–
AlB_2	$V_{ss\sigma}$	$V_{sp\sigma}$	$V_{pp\sigma}$	$V_{pp\pi}$
bond $_{(Al–Al)}$	1.2	–	–	–
bond $_{(B–B\ in\ plane)}$	−2.1	−3.0	1.8	−2.4
bond $_{(B–B\ out\ plane)}$	−0.8	0.0	1.35	−0.15
bond $_{(Al–B)}$	−1.5	−1.5	–	–

Table 2. The on-site energies are obtained by fitting for MgB_2 (Left) and AlB_2 (Right) in units of eV.

On-site energy	MgB_2				AlB_2			
Orbitals	s	p_x	p_y	p_z	s	p_x	p_y	p_z
Mg/Al	3	–	–	–	2	–	–	–
B	−2	0.8	0.8	−0.8	−4.5	−0.3	−0.3	−2.5

dispersion along Γ-A), which is important to establish the magnitude and effects of inter-plane coupling. We find that the slope of σ-bond in the ΓA direction is mainly controlled by $V_{pp\pi}$. Moreover, the larger the absolute value of $V_{pp\pi}$, the greater the slope. This result of $V_{pp\pi}$ is much more profound than just only giving a description of the relationship of ΓA dispersion [36]. In addition, we noticed that the overlap integral values in MgB_2 and AlB_2 are both equal to 0, which is very different from the alone borophene or bilayer borophene within a larger overlap integral values [37,38]. Moreover, the on-site parameters of Mg and B atoms are presented in Table 2. We find the on-site energy in p_x and p_y are equal, which is mainly due to equivalence of the x and y direction.

3.3 Symmetry-Adapted Wannier Functions (SAWF) and effective Hamilton

The QUANTUM ESPRESSO [39,40] package was used to construct SAWF representations by projecting the Bloch states from the first-principles calculations of AlB_2 class's materials onto Mg/Al s and B s, p orbital [41]. It is well known that the band structures of AlB_2 classes are mainly divided into the π-bond and σ-bond. The SAWF fitted band structures are shown in Figure 3. The cyan dashed line is the Fermi level. The π-bond in K and H points are fitted by two p_z orbital of B atoms and the σ-bond in ΓA direction are fitted by the hybrid of sp^2 orbitals of B atoms. The lower is Wannier functions plotted with p_z (π-bond) orbital and sp^2 hybrid (σ-bond) orbitals with one B atom. The red and blue colour represents positive and negative density, respectively. The isosurface is 1.5 e/Å^3. We find from Figure 3 that SAWF fitted bands are very well. Therefore, we can study their properties separately on π-bond and σ-bond by the Wannier Hamilton. More details are shown in Figures S4 and S5.

The essential physics of the DNL structure in AlB_2 classes was characterized by an effective TB model using B p_z orbitals. The p_z bands of AlB_2 classes have a 3D nature, because there is hopping interaction not only among intra-plane B–B bond but also between inter-plane B–B bond. Thus we can construct the spinless effective TB model based on the two B p_z orbitals:

$$H_0(\vec{k}) = \begin{bmatrix} h_{11}(\vec{k}) - \varepsilon & h_{12}(\vec{k}) \\ h_{12}^*(\vec{k}) & h_{22}(\vec{k}) - \varepsilon \end{bmatrix}$$

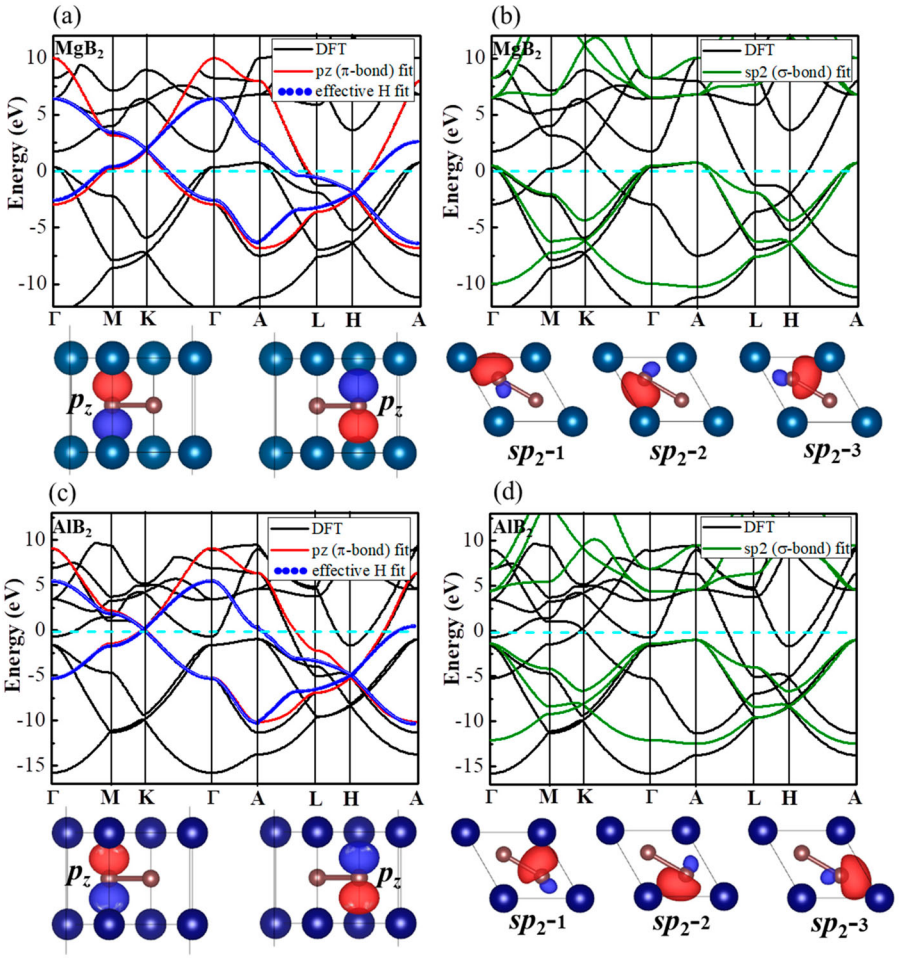

Figure 3. Electronic band structure, the band structure fitted by SAWF and effective Hamiltonian, respectively. (a) The upper are electronic band structure of bulk MgB_2, two p_z orbital (π-bond) SAWF fitted band structure (solid line with red colour) and effective Hamiltonian fitted band structure (dotted line with blue colour). The lower are Wannier functions plotted with p_z (π-bond) orbital. (The cyan dashed line is the Fermi level). (b) The upper are hybrid sp^2 (σ-bond) orbitals SAWF fitted band structure (solid line with olive colour). The lower are Wannier function plotted with sp^2 hybrid (σ-bond) orbitals with one B atom. (c,d) their contents are same as Figure 3 (a,b). (c,d) represents bulk AlB_2. Red and blue colour represents positive and negative density, respectively. The isosurface is 1.5 e/Å^3

where $h_{11}(\vec{k}) = h_{22}(\vec{k}) = 2t_z \cos(ck_z)$, $h_{12}(\vec{k}) = -t(e^{i\vec{k}\cdot\vec{e}_1} + e^{i\vec{k}\cdot\vec{e}_2} + e^{i\vec{k}\cdot\vec{e}_3})$ with $\vec{e}_1 = (0, a/\sqrt{3}, 0)$, $\vec{e}_2 = (-a/2, -a/2\sqrt{3}, 0)$, and $\vec{e}_3 = (a/2, -a/2\sqrt{3}, 0)$; here t and t_z are the absolute value of intra– and inter-plane hopping energy between the nearest-neighbour B p_z orbitals, respectively; here, $\varepsilon = (|\varepsilon_D^H| - |\varepsilon_D^K|)/2$, it represents the average position of two Dirac point. Moreover, $\varepsilon_{MgB_2} = 0.075$ $\varepsilon_{AlB_2} = 2.47$; a is the in-plane lattice constant and c is

the z-direction lattice constant. The calculated effective model band structure is shown in Figure 3(a,c). The model well describes the p_z band structure near and below the Fermi level. Most importantly, we can get the dispersive DNL along the K–H direction. In this effective model without on-site energy correction, the transition k_z point at which the system undergoes an abrupt change from hole to electron doped is absolutely different from first-principle calculations. Moreover, the electron Fermi surfaces with the middle part are shown in Figure S6. The red and blue colours represent the front and back view of the first p_z orbital, respectively. Green and orange colours represent the front and back view of the second p_z orbital, respectively.

3.4 Surface states of the (010) surface

To further reveal the topological nature of the DNL state in AlB_2-type classes, we also calculated the surface states. The surface state spectrum of Mg-terminated (010) of MgB_2 was obtained by an iterative Green's function method [42,43], as shown in Figure 4. The upper part shows the ninth orbital fitted (Mg:s; B:s, p_x, p_y, p_z) projected density of state for the Mg-terminated (010) surface along the cuts at $k_{sy} = 0$, 0.15, 0.3, and 0.5, respectively. The five orbital fitted (Mg:s; B1: p_x, p_z; B2: p_y, p_z) projected density of state for Mg-terminated (010) surface shown in the middle. The lower part shows the two orbital fitted (B1: p_z; B2: p_z) projected density of state for Mg-

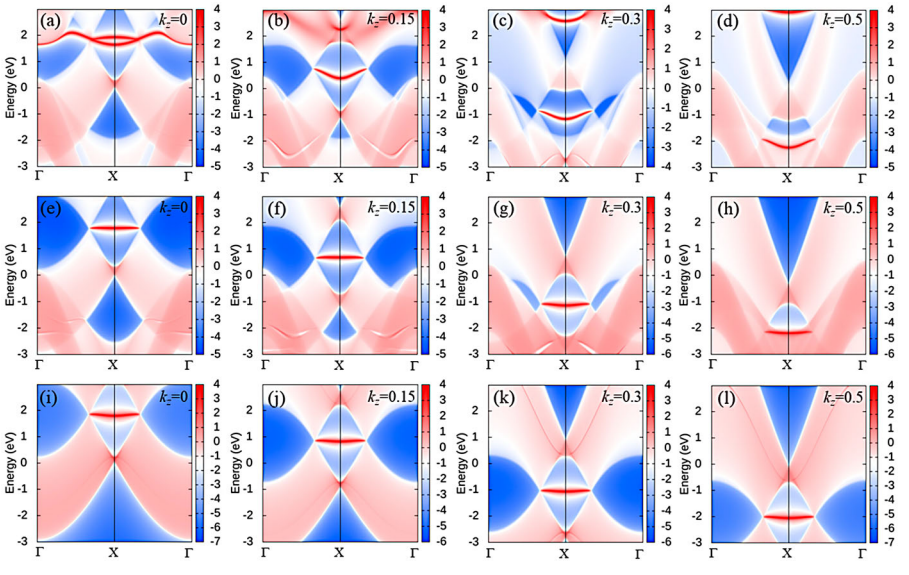

Figure 4. Surface states of the MgB_2 (010) surface. (a–d) The nine orbital fitted (Mg:s; B:s, p_x, p_y, p_z). (e–h) The five orbital fitted (Mg:s; B1: p_x, p_z; B2: p_y, p_z). (i–l) The two orbital fitted (B1: p_z; B2: p_z). The surface states of MgB_2 for Mg-terminated (010) surface along the cuts at $k_{sy} = 0$, 0.15, 0.3, and 0.5, respectively.

terminated (010) surface along the cuts at $k_{sy} = 0$, 0.15, 0.3, and 0.5, respectively. From $k_{sy} = 0$ to $k_{sy} = 0.5$, the Dirac point from K to H points, the surface state also exists. Moreover, the DNLs in HK direction and the corresponding TSS's on the [010] faces are judged by theoretical prediction [12] and experimental confirmation [13]. Furthermore, we find that the degree of bending of the TSS is related to the number of selected orbits, and the more orbits, the stronger the degree of bending. This kind of surface state bending also exists in AlB_2. The surface state spectrums of AlB_2 are shown in Figure 5. Figure 5(a–d) shows the ninth orbital fitted (Al:*s*; B:*s*, p_x, p_y, p_z) projected density of state for Al-terminated (010) surface along the cuts at $k_{sy} = 0$, 0.15, 0.3, and 0.5, respectively. The middle are seven orbital fitted (Al:*s*; B1: p_x, p_y, p_z; B2: p_x, p_y, p_z) projected density of state for Al-terminated (010) surface along the cuts at $k_{sy} = 0$, 0.15, 0.3, and 0.5, respectively. The lower are two orbital fitted (B1: p_z; B2: p_z) projected density of state for Al-terminated (010) surface along the cuts at $k_{sy} = 0$, 0.15, 0.3, and 0.5, respectively. Comparing the surface states of MgB_2 and AlB_2 along the *z*-direction, when $k_z = 0.218$ and $k_z = 0.06$, the surface states fall on the Fermi level. The surface slab bands of MgB_2 and AlB_2 with two p_z orbitals fitted are shown in Figure S7. The left surface state is consistent with the right surface state. The surface slab bands of MgB_2 and AlB_2 with all orbits fitted are shown in Figure S8. The left surface state deviates slightly from the right surface state. The AlB_2 degree of surface state is

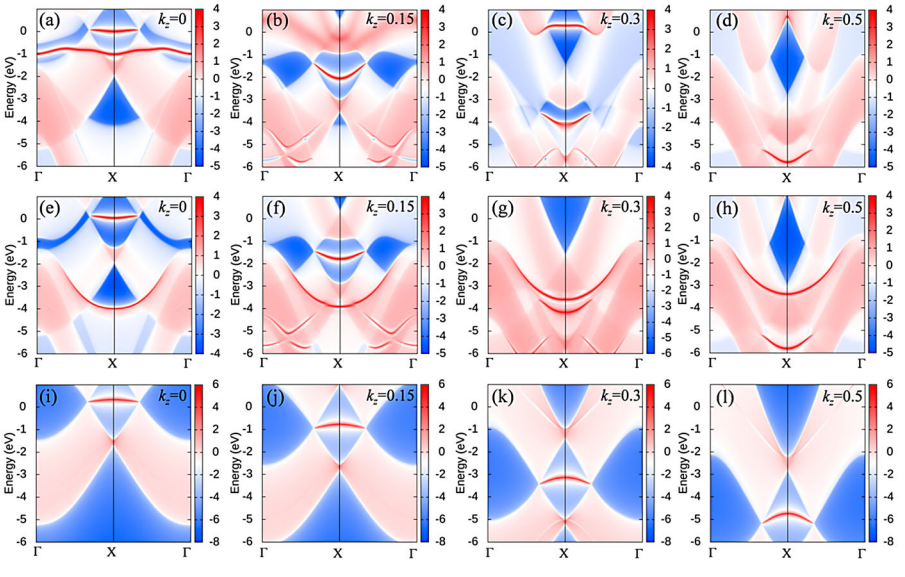

Figure 5. Surface states of the AlB_2 (010) surface. (a–d) The nine orbital fitted (Al:*s*; B:*s*, p_x, p_y, p_z). (e–h) The seven orbital fitted (Al:*s*; B1: p_x, p_y, p_z; B2: p_x, p_y, p_z). (i–l) The two orbital fitted (B1: p_z; B2: p_z). The surface states of AlB_2 for Al-terminated (010) surface along the cuts at $k_{sy} = 0$, 0.15, 0.3, and 0.5, respectively.

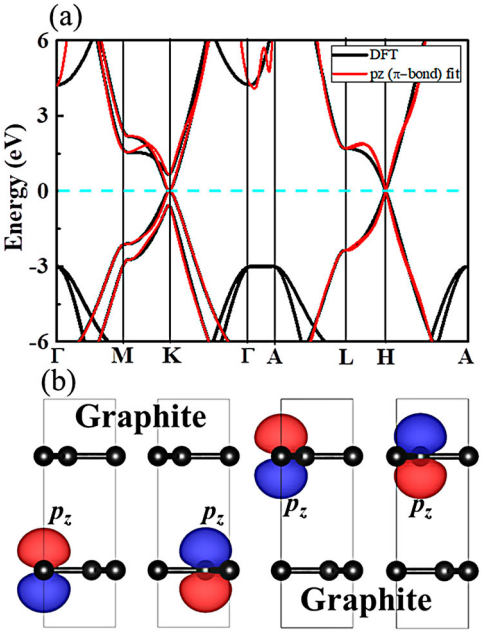

Figure 6. Electronic band structure of Graphite and the Symmetry-Adapted Wannier Functions (SAWF) fitted band structure. (a) The Electronic band structure of Graphite and four p_z orbital (π-bond) Symmetry-Adapted Wannier Functions (SAWF) fitted band structure (solid line with red colour). (The cyan dashed line is the Fermi level). (b) The four p_z Symmetry-Adapted Wannier Functions (SAWF) orbitals. The isosurface is 1.5 e/Å^3

larger than that of MgB_2, which may be due to the energy difference between K and the H points, which demonstrates their degree of symmetry with respect to the Fermi level.

For comparison, we also calculated the band structure of Graphite, which is isoelectronic with MgB_2. The band structures fitted by SAWF by four p_z orbital (π-bond) shown in Figure 6. As shown here, the band fits well near the Fermi level, and the orbitals of adjacent atoms are opposite. In addition, the (010) surface along the cuts at $k_{sy} = 0$, 0.15, 0.3, and 0.5, respectively are shown in Figure 7. Figure 7(a–d) shows the fourth orbital fitted (C: p_z) left surface state along the cuts at $k_{sy} = 0$, 0.15, 0.3, and 0.5, respectively. The fourth orbital fitted (C: p_z) right surface states are shown in Figure 7(e–h). The left surface state is basically the same as the right surface state, which may be due to the fact that the left and right are symmetrical with respect to graphite. Figure 7(i–l) the fourth orbital fitted (C: p_z) slab band structures along the cuts at $k_{sy} = 0$, 0.15, 0.3, and 0.5, respectively. By comparing with graphite, it is convinced that the blending of surface state is mainly affected by some other impurity bands. The essence might come from the asymmetry of the band structure with respect to Fermi level.

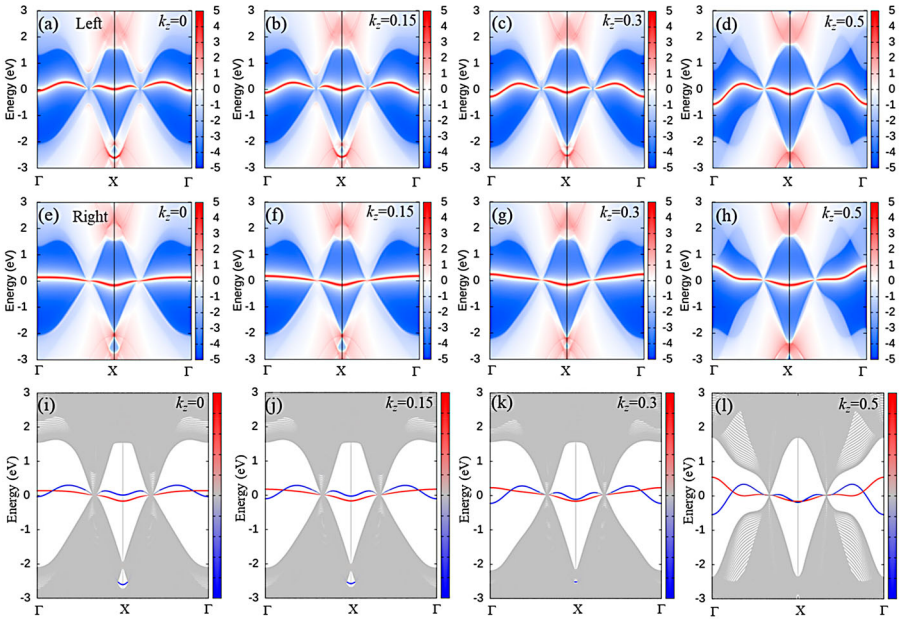

Figure 7. Surface states of the Graphite (010) surface. (a–d) The four orbital fitted (C: p_z) left surface state. (e–h) The four orbital fitted (C: p_z) right surface state. (i–l) The four orbital fitted (C: p_z) slab band structures. The surface states and slab band of Graphite for (010) surface along the cuts at $k_{sy} = 0$, 0.15, 0.3, and 0.5, respectively.

4. Conclusion

In conclusion, based on the first-principles calculations and tight-binding model analysis, we systematically investigate their electronic topological properties of AlB_2-type system. The Slater–Koster method fitted band structure results show that the slope of σ-bond in Γ-A direction is mainly controlled by the absolute value of $V_{pp\pi}$. In addition, the band structure fitted by two p_z SAWF is consistent with the band structure obtained by the effective Hamiltonian of two orbital. In the constructed effective Hamiltonian, since the difference between Fermi level is relative to the Dirac point at the highly symmetrical K and H points, the external on-site energies in MgB_2 and AlB_2 are 0.075 and 2.47 eV, respectively. More strikingly, it can be found that the degree of bending of the TSS. The demonstration of surface state bending changes is similar to the demonstration of energy band inversion in topological insulators. The surface state is always bending, and the more Wannier function orbitals are selected, the higher bending of the surface state. The spin–orbit coupling also always exists in the topological insulator, and the energy band occurs inversion as increasing the strength of spin–orbit coupling. This work provides a theoretical reference for the exploration the topological property of DNL in AlB_2-type topological superconductivity materials.

Acknowledgements

We would like to thank Jia-Tao Sun and Hu Xu for helpful discussions. C. Cheng acknowledges financial support from National Natural Science Foundation of China (Grant No. 11904244) and China Postdoctoral Science Foundation (Grant No. 2020M683276). We also acknowledge the computing resources from the High Performance Computing Center of Sichuan Normal University.

Disclosure statement

No potential conflict of interest was reported by the author(s).

Funding

We acknowledge financial support from National Natural Science Foundation of China (grant number 11904244) and China Postdoctoral Science Foundation (grant number 2020M683276).

ORCID

Cai Cheng http://orcid.org/0000-0002-1331-539X

References

[1] C.L. Kane and E.J. Mele, *Z_2 topological order and the quantum spin Hall effect*. Phys. Rev. Lett. 95 (2005), pp. 146802.
[2] M.Z. Hasan and C.L. Kane, *Colloquium: topological insulators*. Rev. Mod. Phys. 82 (2010), pp. 3045.
[3] X.-L. Qi and S.-C. Zhang, *Topological insulators and superconductors*. Rev. Mod. Phys. 83 (2011), pp. 1057–1110.
[4] N.P. Armitage, E.J. Mele and A. Vishwanath, *Weyl and Dirac semimetals in three-dimensional solids*. Rev. Mod. Phys. 90 (2018), pp. 015001.
[5] T. Zhang, Z. Song, A. Alexandradinata, H. Weng, C. Fang, L. Lu and Z. Fang, *Double-Weyl Phonons in transition-metal monosilicides*. Phys. Rev. Lett. 120 (2018), pp. 016401.
[6] H. Miao, T.T. Zhang, L. Wang, D. Meyers, A.H. Said, Y.L. Wang, Y.G. Shi, H.M. Weng, Z. Fang and M.P.M. Dean, *Observation of Double Weyl Phonons in parity-breaking FeSi*. Phys. Rev. Lett. 121 (2018), pp. 035302.
[7] Y. Jin, R. Wang and H. Xu, *Recipe for Dirac phonon states with a quantized valley berry phase in Two-dimensional hexagonal lattices*. Nano Lett. 18 (2018), pp. 7755–7760.
[8] B.W. Xia, R. Wang, Z.J. Chen, Y.J. Zhao and H. Xu, *Symmetry-protected ideal type-II Weyl Phonons in CdTe*. Phys. Rev. Lett. 123 (2019), pp. 065501.
[9] R. Wang, B.W. Xia, Z.J. Chen, B.B. Zheng, Y.J. Zhao and H. Xu, *Symmetry-protected topological triangular Weyl complex*. Phys. Rev. Lett. 124 (2020), pp. 105303.
[10] J. Nagamatsu, N. Nakagaua, T. Muranaka, Y. Zenitani and J. Akimitsu, *Superconductivity at 39 K in magnesium diboride*. Nature 410 (2001), pp. 632001.
[11] S.L. Bud'ko, G. Lapertot, C. Petrovic, C.E. Cunningham, N. Anderson and P.C. Canfield, *Boron isotope effect in superconducting MgB_2*. Phys. Rev. Lett. 86 (2001), pp. 1877.

[12] K.-H. Jin, H. Huang, J.-W. Mei, Z. Liu, L.-K. Lim and F. Liu, *Topological superconducting phase in high-Tc superconductor MgB2 with dirac–nodal-line fermions*. NPJ Comput. Mater. 5 (2019), pp. 57.
[13] X. Zhou, K.N. Gordon, K.H. Jin, H. Li, D. Narayan, H. Zhao, H. Zheng, H. Huang, G. Cao, N.D. Zhigadlo, F. Liu and D.S. Dessau, *Observation of topological surface state in high temperature superconductor MgB_2*. Phys. Rev. B. 100 (2019), pp. 184511.
[14] D. Takane, S. Souma, K. Nakayama, T. Nakamura, H. Oinuma, K. Hori, K. Horiba, H. Kumigashira, N. Kimura, T. Takahashi and T. Sato, *Observation of a Dirac nodal line in AlB_2*. Phys. Rev. B. 98 (2018), pp. 041101(R).
[15] X. Feng, C. Yue, Z. Song, Q. Wu and B. Wen, *Topological Dirac nodal-net fermions in AlB_2-type TiB_2 and ZrB_2*. Phys. Rev. Mater. 2 (2018), pp. 014202.
[16] R. Li, H. Ma, X. Cheng, S. Wang, D. Li, Z. Zhang, Y. Li and X.Q. Chen, *Dirac node lines in pure alkali earth metals*. Phys. Rev. Lett. 117 (2016), pp. 096401.
[17] Z. Cheng, Z. Zhang, H. Sun, S. Li, H. Yuan, Z. Wang, Y. Cao, Z. Shao, Q. Bian, X. Zhang, F. Li, J. Feng, S. Ding, Z. Mao and M. Pan, *Visualizing Dirac nodal-line band structure of topological semimetal ZrGeSe by ARPES*. APL Mater. 7 (2019), pp. 051105.
[18] Y. Xu, Y. Gu, T. Zhang, C. Fang, Z. Fang, X.-L. Sheng and H. Weng, *Topological nodal lines and hybrid Weyl nodes in $YCoC_2$*. APL Mater. 7 (2019), pp. 101109.
[19] Y. Shao, Z. Sun, Y. Wang, C. Xu, R. Sankare, A.J. Breindel, C. Cao, M.M. Fogler, A.J. Millis, F. Chou, Z. Li, T. Timusk, M.B. Maple and D.N. Basov, *Optical signatures of Dirac nodal lines in $NbAs_2$*. Proc. Natl. Acad. Sci. U.S.A. 116 (2019), pp. 1168.
[20] M. Tian, J. Wang, X. Liu, W. Chen, Z. Liu, H. Du, X. Ma, X. Cui, A. Zhao, Q. Shi, Z. Wang, Y. Luo, J. Yang, B. Wang and J.G. Hou, *Creation of the Dirac Nodal Line by extrinsic Symmetry engineering*. Nano Lett. 20 (2020), pp. 2157–2162.
[21] Z. Liu, R. Lou, P. Guo, Q. Wang, S. Sun, C. Li, S. Thirupathaiah, A. Fedorov, D. Shen, K. Liu, H. Lei and S. Wang, *Experimental observation of Dirac Nodal links in centrosymmetric semimetal TiB_2*. Phys. Rev. X. 8 (2018), pp. 031044.
[22] J. Li, Q. Xie, J. Liu, R. Li, M. Liu, L. Wang, D. Li, Y. Li and X.-Q. Chen, *Phononic Weyl nodal straight lines in MgB_2*. Phys. Rev. B. 101 (2020), pp. 024301.
[23] J.A. Alarco, P.C. Talbot and I.D.R. Mackinnon, *Phonon anomalies predict superconducting T_c forAlB_2-type structures*. Phys. Chem. Chem. Phys. 17 (2015), pp. 25090.
[24] C. Cheng, M.Y. Duan, Z. Wang and X.L. Zhou, *Alb_2 and MgB_2: a comparative study of their electronic, phonon and superconductivity properties via first principles*. Philos. Mag. 100 (2020), pp. 2275–2289.
[25] G. Kresse and J. Hafner, *Ab initio molecular dynamics for liquid metals*. Phys. Rev. B. 47 (1993), pp. 558.
[26] G. Kresse and J. Hafner, *Ab initio molecular-dynamics simulation of the liquid-metal–amorphous-semiconductor transition in germanium*. Phys. Rev. B. 49 (1994), pp. 14251.
[27] G. Kresse and J. Furthmüller, *Efficient iterative schemes for ab initio total-energy calculations using a plane-wave basis set*. Phys. Rev. B. 54 (1996), pp. 11169–11186.
[28] P.E. Blöchl, *Projector augmented-wave method*. Phys. Rev. B. 50 (1994), pp. 17953–17979.
[29] J.P. Perdew, J.A. Chevary, S.H. Vosko, K.A. Jackson, M.R. Pederson, D.J. Singh and C. Fiolhais, *Atoms, molecules, solids, and surfaces-applications of the generalized gradient approximation for exchange and correlation*. Phys. Rev. B. 46 (1992), pp. 6671.
[30] Q. Wu, S. Zhang, H.-F. Song, M. Troyer and A.A. Soluyanov, *Wanniertools: An open-source software package for novel topological materials*. Comput. Phys. Commun. 224 (2018), pp. 405–416.

[31] M. d'Astuto, R. Heid, B. Renker, F. Weber, H. Schober, O. De la Peña-Seaman, J. Karpinski, N.D. Zhigadlo, A. Bossak and M. Krisch, *Nonadiabatic effects in the phonon dispersion of $Mg_{1-x}Al_xB_2$*. Phys. Rev. B. 93 (2016), pp. 180508(R).
[32] J.A. Alarco, P.C. Talbotab and I.D.R. Mackinnon, *Coherent phonon decay and the boron isotope effect for MgB_2*. Phys. Chem. Chem. Phys. 16 (2014), pp. 25386.
[33] J.C. Slater and G.F. Koster, *Simplified LCAO method for the periodic potential problem*. Phys. Rev. 94 (1954), pp. 1498.
[34] https://tight-binding.com/.
[35] M. Nakhaee, S.A. Ketabi and F.M. Peeters, *Tight-Binding Studio: a technical software package to find the parameters of tight-binding Hamiltonian*. Comput. Phys. Commun. 254 (2020), pp. 107379.
[36] J.M. An and W.E. Pickett, *Superconductivity of MgB_2: covalent bonds driven metallic*. Phys. Rev. Lett. 86 (2001), pp. 4366.
[37] M. Nakhaee, S.A. Ketabi and F.M. Peeters, *Tight-binding model for borophene and borophane*. Phys. Rev. B. 97 (2018), pp. 125424.
[38] M. Nakhaee, S.A. Ketabi and F.M. Peeters, *Dirac nodal line in bilayer borophene: tight-binding model and low-energy effective Hamiltonian*. Phys. Rev. B. 98 (2018), pp. 115413.
[39] P. Giannozzi, S. Baroni, N. Bonini, M. Calandra, R. Car, C. Cavazzoni, D. Ceresoli, G.L. Chiarotti, M. Cococcioni, I. Dabo, A. Dal Corso, S. Fabris, G. Fratesi, S. de Gironcoli, R. Gebauer, U. Gerstmann, C. Gougoussis, A. Kokalj, M. Lazzeri, L. Martin-Samos, N. Marzari, F. Mauri, R. Mazzarello, S. Paolini, A. Pasquarello, L. Paulatto, C. Sbraccia, S. Scandolo, G. Sclauzero, A.P. Seitsonen, A. Smogunov, P. Umari and R.M. Wentzcovitch, *QUANTUM ESPRESSO: a modular and open-source software project for quantum simulations of materials*. J. Phys.: Condens. Matter. 21 (2009), pp. 395502.
[40] P. Giannozzi, O. Andreussi, T. Brumme, O. Bunau, M. Buongiorno Nardelli, M. Calandra, R. Car, C. Cavazzoni, D. Ceresoli, M. Cococcioni, N. Colonna, I. Carnimeo, A. Dal Corso, S. de Gironcoli, P. Delugas, R.A. DiStasio Jr, A. Ferretti, A. Floris, G. Fratesi, G. Fugallo, R. Gebauer, U. Gerstmann, F. Giustino, T. Gorni, J. Jia, M. Kawamura, H.-Y. Ko, A. Kokalj, E. Küçükbenli, M. Lazzeri, M. Marsili, N. Marzari, F. Mauri, N.L. Nguyen, H.-V. Nguyen, A. Otero-de-la-Roza, L. Paulatto, S. Poncé, D. Rocca, R. Sabatini, B. Santra, M. Schlipf, A.P. Seitsonen, A. Smogunov, I. Timrov, T. Thonhauser, P. Umari, N. Vast, X. Wu and S. Baroni, *Advanced capabilities for materials modelling with quantum ESPRESSO*. J. Phys.: Condens. Matter. 29 (2017), pp. 465901.
[41] A.A. Mostofi, J.R. Yates, G. Pizzi, Y.-S. Lee, I. Souza, D. Vanderbilt and N. Marzari, *An updated version of wannier90: A tool for obtaining maximally-localised Wannier functions*. Comput. Phys. Commun. 185 (2014), pp. 2309–2310.
[42] M.L. Sancho, J.L. Sancho and J. Rubio, *Quick iterative scheme for the calculation of transfer matrices: application to Mo (100)*. J. Phys. F: Met. Phys. 14 (1984), pp. 1205.
[43] M.L. Sancho, J.L. Sancho and J. Rubio, *Highly convergent schemes for the calculation of bulk and surface Green functions*. J. Phys. F: Met. Phys. 15 (1985), pp. 851.